JOC The Journal of Organic Chemistry

Article

pubs.acs.org/joc

Benzo- and Naphthopentalenes: Syntheses, Structures, and Properties

Shin-ichiro Kato, Satoshi Kuwako, Nobutaka Takahashi, Tomokazu Kijima, and Yosuke Nakamura*

Division of Molecular Science, Faculty of Science and Technology, Gunma University, 1-5-1 Tenjin-cho, Kiryu, Gunma 376-8515, Japan

Supporting Information

ABSTRACT: Benzo- and naphthopentalene derivatives were synthesized, and the effects of structural variations on their antiaromaticity and optoelectronic and electrochemical properties were examined experimentally and theoretically in detail. The results unveiled that with increasing the bond order of the carbon−carbon bond ([5,6] junction) shared by the pentalene and aromatic moieties, the 8π antiaromatic character of pentalene is enhanced and the HOMO−LUMO gap is decreased, which accompanies both the elevation of the HOMO level and the lowering of the LUMO level. The ethynylene units between the pentalene skeleton and the phenyl groups proved to extend π-conjugation sufficiently.

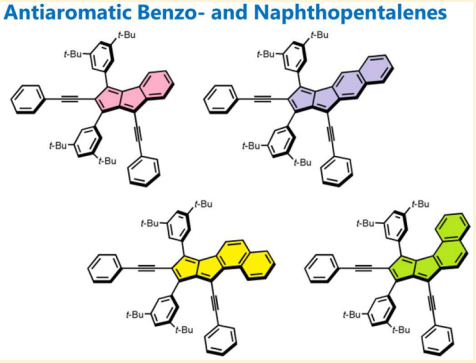

INTRODUCTION

Polycyclic conjugated hydrocarbons (PCHs) are ubiquitous structures in the field of organic and molecular electronics, and thus, long-term attention has been paid to a variety of aromatic PCH scaffolds, especially acene-, phene-, and rylene-type hydrocarbons.[1] The tremendous synthetic study on aromatic PCHs has provided useful, predictive knowledge about structure−π-conjugative property relationships in these families over the past decades.

The Hückel antiaromatic compounds with 4$n\pi$ electronic structures usually have a high HOMO level and low LUMO level, namely, a small HOMO−LUMO gap relative to aromatic compounds with [4n + 2]π electronic structures.[2,3] These characteristics of antiaromatic compounds are favorable for release and/or acceptance of electrons and absorption of light in the visible and/or near-infrared (NIR) regions. Although antiaromatic compounds are considerably unstable in general, the annulation of aromatic ring systems effectively increases the stability and enables them to be handled without special precautions. Therefore, antiaromatic PCHs have recently attracted interest as promising materials of an active layer in optoelectronic devices such as organic field-effect transistors (OFETs) and organic photovoltaics (OPVs).[4,5]

Pentalene, which is composed of two fused cyclopentadiene rings with 8π electrons, is one of the most important antiaromatic compounds.[6,7] Although pentalene itself is thermally unstable and dimerizes above −196 °C, dibenzo[a,e]pentalene is a fairly stable compound.[8] In 2009, Kawase's group and Tilley's group independently reported the efficient synthesis of substituted dibenzo[a,e]pentalene derivatives by nickel-mediated and palladium-catalyzed dimerization of o-alkynylhaloarenes, respectively,[9−11] and the former group revealed the unique structural and electronic properties of a series of dibenzo[a,e]pentalenes. After these impressive works, investigation on the synthesis and properties of various bisannulated[a,e]pentalenes, in which the pentalene core is fused with two benzoid aromatic ring systems, has been a topic of intense interest;[12−20] it was demonstrated that some compounds showed high charge mobilities.[12,18,19b,20]

In 1967, Ried and Freitag synthesized benzopentalene derivative **1** (Chart 1), which was the first member of monoannulated pentalene derivatives;[21] the synthesis of **1** is shown in Scheme S1 in the Supporting Information. Examination of the synthesis and properties of monoannulated pentalenes should be a meaningful task in pentalene chemistry, because they are considered to possess the antiaromaticity and properties that greatly reflect the parent pentalene 8π electron system when compared to bisannulated[a,e]pentalenes. The generation of parent benzopentalene using flash vacuum pyrolysis was reported by several research groups;[22−27] however, little attention was paid to monoannulated pentalenes. Very recently, Diederich and co-workers reported facile access to various benzo- and naphthopentalene derivatives by cascade carbopalladation reaction of *gem*-dibromoolefins and alkynes[28] and disclosed that monoannulated pentalene derivatives exhibit high antiaromatic character, small HOMO−LUMO gaps, and enhanced amphoteric redox behavior compared to bisannulated analogues. Nevertheless, monoannulated pentalenes are still less explored than bisannulated[a,e]pentalenes to date, and there is plenty of room to study the structure−property relationships of well-defined monoannulated pentalenes.

Received: June 11, 2016
Published: July 28, 2016

DOI: 10.1021/acs.joc.6b01409
J. Org. Chem. 2016, 81, 7700−7710

Chart 1. Benzo- and Naphthopentalenes 1−6

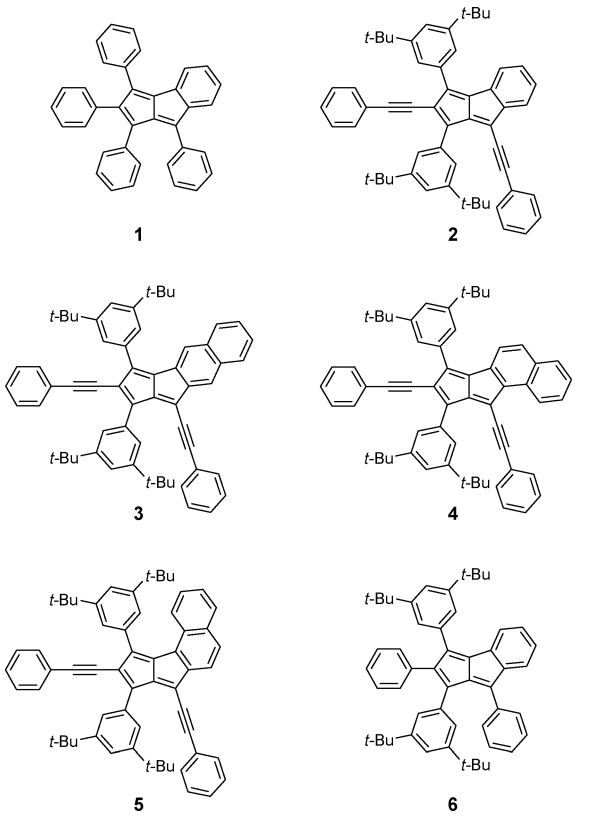

The elucidation of the relationships of structure, antiaromaticity, and frontier molecular orbital levels, in particular, HOMO and LUMO levels, in conjugated polycycles embedding an antiaromatic unit is an important subject from the viewpoint of the deepened understanding of antiaromatic (aromatic) behavior as well as the design of compounds with bespoke electronic properties.[12,29−32] In this regard, we were motivated to synthesize higher congeners of **1**, namely, benzo- and naphthopentalene derivatives **2**−**5** (Chart 1). We envisioned that the comparison of the structures and physicochemical properties of **2**−**5** together with reference compound **6** would give crucial insights into the factors (i.e., the ethynylene units, the aromatic rings annulated to the pentalene moiety, and their fusion position and orientation) that govern the antiaromaticity and properties. In **2**−**6**, we decided to introduce the *t*-Bu groups in terms of solubility and crystallinity. In this article, we demonstrate detailed research on the synthesis, structural features, antiaromaticity, and optoelectronic and electrochemical properties of **2**−**6** by means of X-ray crystallographic analyses, quantum chemical calculations, electronic absorption spectroscopy, and electrochemistry.

RESULTS AND DISCUSSION

Synthesis. The synthetic route to benzo- and naphthopentalenes **2**−**5** is outlined in Scheme 1.[33] First, we subjected ninhydrin derivatives **8**−**10** to the aldol condensation with 1,3-bis(3,5-di-*tert*-butylphenyl)propan-2-one (**7**) in the presence of tetrabutylammonium hydroxide (TBAOH) as a base to prepare the corresponding pentalenequinones **11**−**14**, which are key intermediates in the synthesis of **2**−**5**. Gratifyingly, the two isomers **13** and **14** produced by the reaction of **10** and **19** were readily separated by conventional silica gel column chromatography; the structures of **13** and **14** were unambiguously identified through the use of 2D NMR (NOESY, HMBC) experiments (Figures S38−S44 in the Supporting Information). Then nucleophilic addition of the lithium acetylide of phenylacetylene to **11**−**14** gave the corresponding diols **15**−**18**,[34] which were finally subjected to $SnCl_2{\cdot}2H_2O$-mediated reduction to furnish pentalenes **2**−**5**. Compound **6** was obtained in similar synthetic procedures to **1** as shown in Scheme S2 in the Supporting Information. Pentalenes **2**−**6** were fully characterized by various spectroscopic methods. They gave well-resolved ^{1}H NMR spectra in $CDCl_3$ at room temperature, indicating negligible biradicaloid behavior. All of **2**−**6** are reasonably soluble in common organic solvents such as toluene, CH_2Cl_2, and acetone and stable in both solution and the solid state at room temperature under air.

Structural Properties. The structures of **2**−**5** were verified by X-ray crystallographic analyses as shown in Figure 1; in the crystal of **3**, there are two crystallographically independent molecules (abbreviated as $\mathbf{3}_1$ and $\mathbf{3}_2$) in the unit cell. The benzo- and naphthopentalene skeletons of **2**−**5** have a highly planar geometry with the deviation from their mean planes of less than 0.116 Å. The dihedral angles between the pentalene moiety and the phenyl groups via the ethynylene units are 11.6−48.7°, and the ethynylene units are distorted with bond angles of 166.5−177.8°.

In all of the crystal structures, the C3−C4, C5−C6, and C7−C8 bond lengths are surely shorter than the C1−C2, C1−C8, C2−C3, C4−C5, and C6−C7 bond lengths, illustrating double- and single-bond alternations in the pentalene moieties, characteristic for antiaromatic compounds; similar bond length alternation is observed in monoannulated pentalene derivatives synthesized by Diederich and co-workers.[28] It is worth stating that **2**−**5** considerably differ in the bond lengths ($\alpha_{X\text{-ray}}$) of the C1−C2 bond ([5,6] junction) shared by the pentalene and aromatic moieties to each other, and thus, the $\alpha_{X\text{-ray}}$ values decrease in order of **3** (1.427(4), 1.436(4) Å) > **2** (1.412(3) Å) > **4** (1.399(6) Å) ≈ **5** (1.3947(17) Å). This finding illustrates that the trend for the bond order of the [5,6] junction appears to be **3** < **2** < **4** ≈ **5**,[35,36] which should be attributed to the fact that the bond order of carbon−carbon bonds of benzene and naphthalene follows the trend of the 2−3 bond of naphthalene < the bond of benzene < the 1−2 bond of naphthalene. In **2**, $\mathbf{3}_1$, and $\mathbf{3}_2$, the C1−C9 and C2−C10 bonds are considerably shorter than the C1−C2 bond, and thus, these molecules possess *exo*-butadiene conjugation with regard to the pentalene skeleton as depicted in Chart 1. On the other hand, in **4** the C1−C9, C2−C10, and C1−C2 bond lengths are roughly similar to each other, and instead, in **5** the C1−C9 and C2−C10 bonds are slightly longer than the C1−C2 bond. Overall, detailed examination on the bond lengths in **2**−**5** strongly suggests that the contribution of the pentalene 8π electron system to the electronic properties becomes large in the following order: **3** < **2** < **4** ≈ **5**. Effective π−π interactions are observable between the neighboring molecules in the crystal packing of **3**−**5** (Figure S6), whereas almost no noticeable π−π interaction is observed in the packing diagram of **2**.

To gain further insight into the molecular structures of **2**−**5** as well as **6**, we optimized their ground-state structures by density functional theory (DFT) calculations using the Gaussian 09 program package (Figures S13 and S14).[36] The selected geometrical parameters at the PBE0/6-31G(d) level of theory are given in Tables S3−S12. We noticed that the optimized structures of **2**−**5** with the PBE0 and M06 methods

DOI: 10.1021/acs.joc.6b01409
J. Org. Chem. 2016, 81, 7700−7710

Scheme 1. Synthesis of Benzo- and Naphthopentalenes 2−5[a]

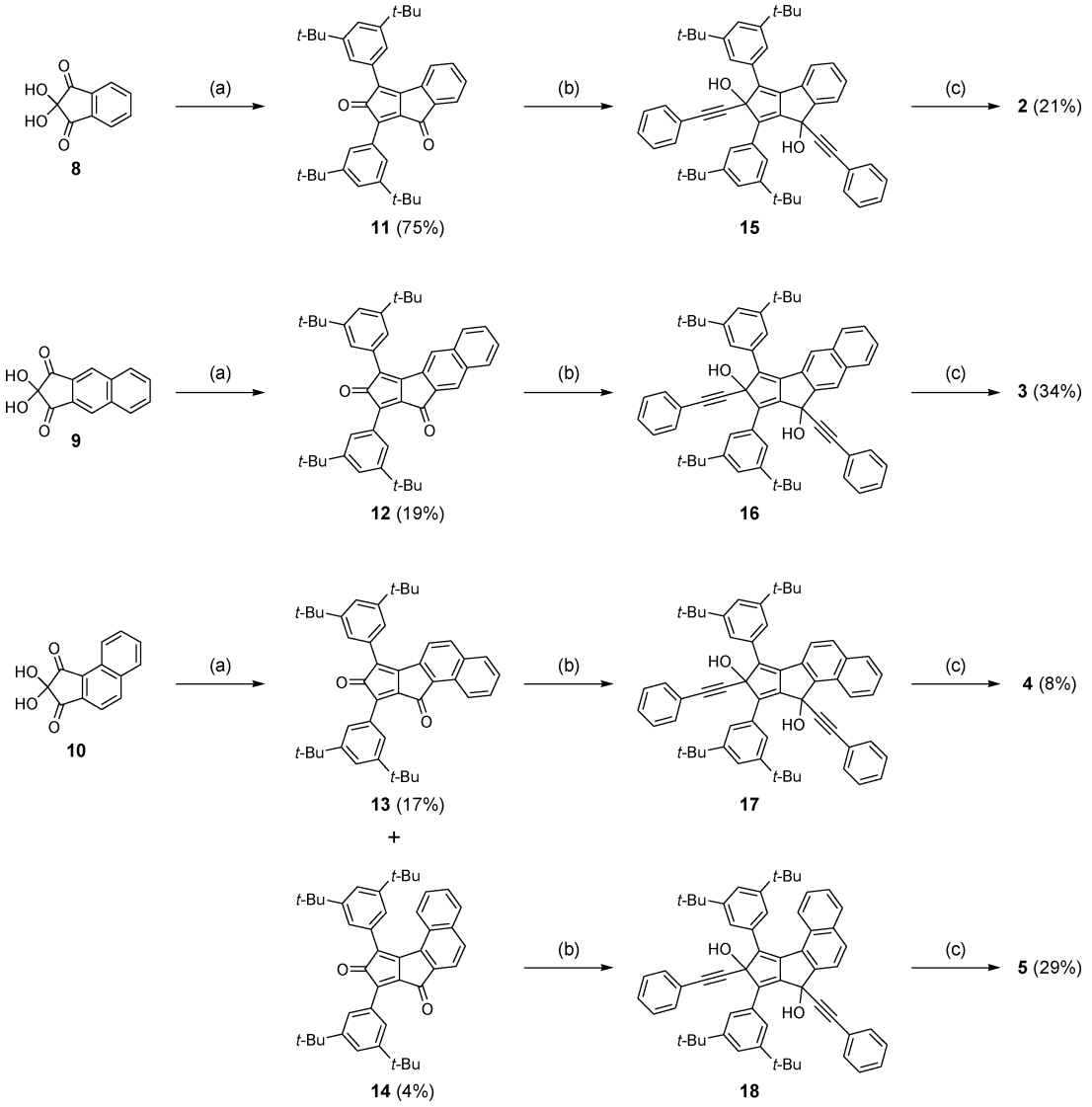

[a]Reagents and conditions: (a) 1,3-bis(3,5-di-*tert*-butylphenyl)propan-2-one (**7**), TBAOH, 75 °C in EtOH (for **8**) or 95 °C in 1-butanol (for **9** and **10**); (b) PhC≡CLi, −78 °C to RT in Et_2O (for **11**), RT in Et_2O/benzene (for **12**), or −78 °C to RT in THF (for **13** and **14**); (c) $SnCl_2{\cdot}2H_2O$, 45 °C in THF. The yields for **2**−**5** are based on the corresponding **11**−**14**. The synthetic scheme of **6** is shown in Scheme S2 in the Supporting Information.

reasonably agreed well with the corresponding X-ray structures with regard to the bond lengths; these methods reproduced the experimental data better than the B3LYP and CAM-B3LYP methods (Tables S3−S12). The PCH frameworks in the optimized structures of **2**−**4** are planar, as is true with the crystallographic results. Unlike the crystal structure of **5**, the naphthopentalene skeleton in the optimized **5** is slightly twisted (Figure S14d), presumably due to the steric repulsion between the naphthalene ring and the adjacent 3,5-di-*tert*-butylphenyl group. This finding suggests that the crystal packing force significantly contributes to the planar naphthopentalene structure of **5** in the solid state; **5** forms the stacked dimer structure through effective $\pi-\pi$ stacking interactions between the naphthopentalene moieties (Figure S6d). The benzopentalene skeleton in the optimized structure of **6** is planar. The dihedral angles between the pentalene moiety and the attached phenyl groups (ca. 50°) in **6** are evidently larger than those in **2**−**5** (ca. 15°−25°). The calculated C1−C2 bond lengths (α_{calcd}) of **2**−**5** decrease in the order of **3** (1.442 Å) > **2** (1.419 Å) > **4** (1.406 Å) ≈ **5** (1.404 Å), and thus, the trend of α_{calcd} values of **2**−**5** is consistent with that of $\alpha_{X\text{-}ray}$ values (vide supra). The α_{calcd} value of **6** (1.427 Å) is similar to that of **2**, suggesting only a marginal effect of the ethynylene units on the C1−C2 bond lengths.

Antiaromaticity. The nucleus-independent chemical shifts (NICS) calculations are convincing and widely used to investigate the tropicity of π-conjugated cyclic systems.[37] The recently established NICS-XY-scan, where the NICS values are plotted over the entire molecule, allows for the evaluation of the local/global tropicity of PCHs. We calculated $NICS(1.7)_{\pi ZZ}$ values of **2**−**5**, whose geometries were derived from their crystal structures, based on the NICS-XY-scan and σ-only model[38] at the GIAO-B3LYP/6-311+G(d,p) level of theory using the Aroma package;[39] the σ-only model was only applied to the benzo- and naphthopentalene moieties to reduce the calculation time.

DOI: 10.1021/acs.joc.6b01409
J. Org. Chem. 2016, 81, 7700−7710

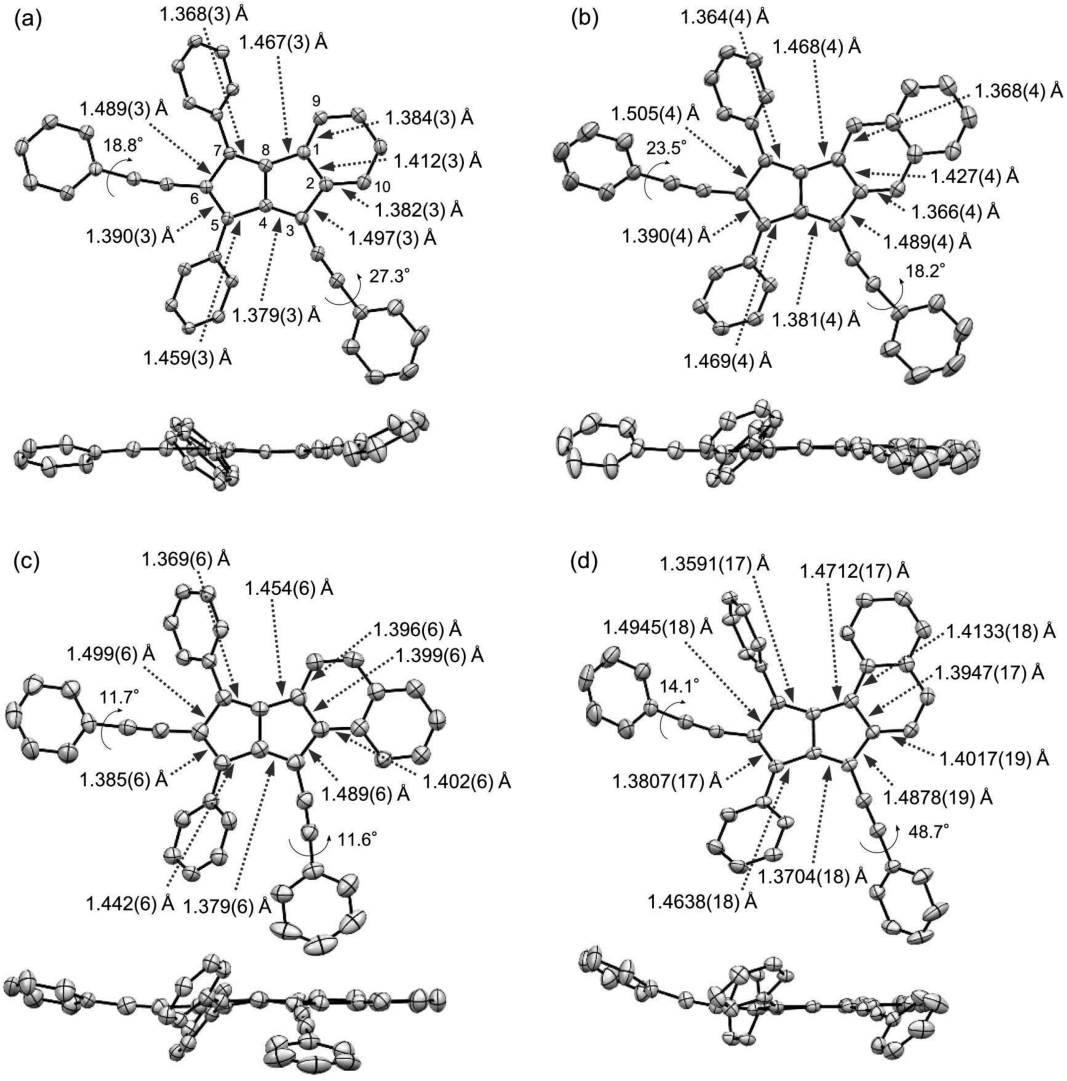

Figure 1. X-ray crystal structures of (a) **2**, (b) $\mathbf{3}_1$, (c) **4**, and (d) **5** of bird-eye view (top) and side view (bottom). Displacement ellipsoids are shown at the 50% probability level. Hydrogen atoms and *t*-Bu groups are omitted for clarity. One of the two independent molecules for **3** is shown.

As shown in Figure 2, the NICS(1.7)$_{\pi ZZ}$ values of the two 5-membered rings A and B of **2**−**5** are unexceptionally positive, indicating semilocal paratropic ring currents at the 8π electron circuit of the pentalene moiety. The 6-membered rings C next to the 5-membered rings B display negative NICS(1.7)$_{\pi ZZ}$ values; however, these values are obviously less negative than those of benzene and naphthalene (ca. −16).[38c] This implies semiglobal paratropic ring currents at the 12π electron circuit of the 5−5−6-membered ring subunits. The outer 6-membered rings D of **3**−**5** show almost the same NICS(1.7)$_{\pi ZZ}$ values as that of naphthalene, indicating virtually no global paratropic ring current at the 16π electron perimeter.[40,41]

Pentalene **2** displays the NICS(1.7)$_{\pi ZZ}$ values for the 5-membered rings A and B to be +16.2 and +11.9, respectively. The NICS(1.7)$_{\pi ZZ}$ values for rings A and B of $\mathbf{3}_1$ and $\mathbf{3}_2$ are less positive than those of **2** ($\mathbf{3}_1$ = +10.9 (A), +7.5 (B); $\mathbf{3}_2$ = +12.3 (A), + 9.1 (B)), while the values of both **4** and **5** are considerably positive relative to those of **2** (**4** = +22.0 (A), +18.9 (B); **5** = +22.6 (A), +19.2 (B)). This demonstrates that the semilocal 8π antiaromatic character of the pentalene moiety of **2**−**5** becomes strong in order of **3** < **2** < **4** ≈ **5** (Figure S18). Thus, the annulation at the 2,3 positions of naphthalene to the pentalene moiety decreases the antiaromaticity relative to the benzannulation, while that at the 1,2 positions enhances the antiaromaticity;[42] the effect of the orientation of the naphthalene ring with respect to the pentalene moiety on the antiaromaticity seems to be negligible. Figure 3 shows the plot of the average (abbreviated as NICS(1.7)$_{\pi ZZ}^{\text{avg.(X-ray)}}$) of the NICS(1.7)$_{\pi ZZ}$ values for rings A and B of **2**−**5** against the $\alpha_{\text{X-ray}}$ values. The strong dependence of the antiaromaticity for the pentalene moiety of **2**−**5** on the bond order of the [5,6] junction is manifested by the linear correlation between the NICS(1.7)$_{\pi ZZ}^{\text{avg.(X-ray)}}$ and $\alpha_{\text{X-ray}}$ values. Therefore, it is reasonable to assume that the decrease in the bond length of the [5,6] junction, namely, the increase in the bond order, augments the 8π electronic character of pentalene and thus enhances the antiaromaticity.

We also performed NICS calculations for **2**−**6** through NICS-XY-scans with the use of their DFT-optimized geometries (Figure S17). The average (abbreviated as NICS(1.7)$_{\pi ZZ}^{\text{avg.(calcd)}}$) of the NICS(1.7)$_{\pi ZZ}$ values for rings A and B of the optimized **2**−**5** was found to increase in order of **3** (+10.5) < **2** (+14.4) < **5** (+19.1) ≈ **4** (+19.8), and thus, this trend is in good agreement with that of the

DOI: 10.1021/acs.joc.6b01409
J. Org. Chem. 2016, 81, 7700−7710

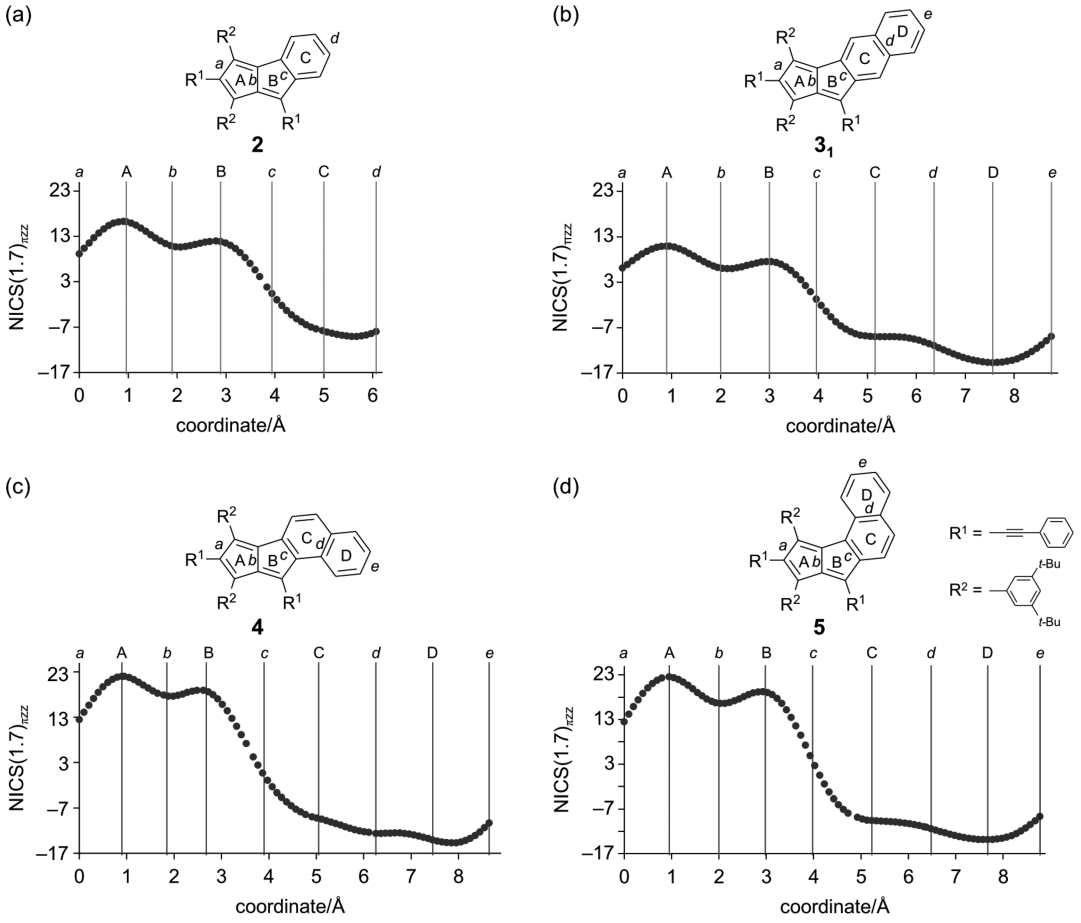

Figure 2. NICS-XY-scan results (NICS(1.7)$_{\pi zz}$) of (a) **2**, (b) $\mathbf{3}_1$, (c) **4**, and (d) **5** at the GIAO-B3LYP/6-311+G(d) based on the X-ray structures. Uppercase and lowercase characters denote ring and bond, respectively.

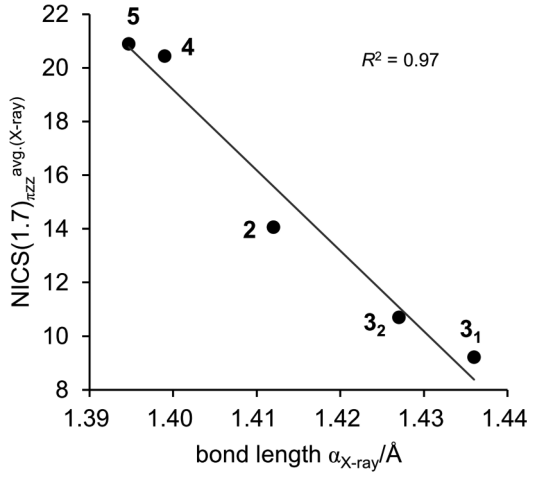

Figure 3. Plot of NICS(1.7)$_{\pi zz}^{\text{avg.(X-ray)}}$ values as a function of $\alpha_{\text{X-ray}}$ values of **2**, $\mathbf{3}_1$, $\mathbf{3}_2$, **4**, and **5**: $\alpha_{\text{X-ray}}$ values are derived from the crystal structures. NICS(1.7)$_{\pi zz}^{\text{avg.(X-ray)}}$ is defined as the average of the NICS(1.7)$_{\pi zz}$ values for rings A and B. Two independent molecules for **3** in the unit cell are abbreviated as $\mathbf{3}_1$ and $\mathbf{3}_2$.

NICS(1.7)$_{\pi ZZ}^{\text{avg.(X-ray)}}$ values; the NICS(1.7)$_{\pi ZZ}^{\text{avg.(calcd)}}$ values are apparently proportional to the α_{calcd} values (Figures S18 and S19). Compound **6** shows almost the same NICS(1.7)$_{\pi ZZ}^{\text{avg.(calcd)}}$ value (+15.2) as that of **2**, probably reflecting the fact that the α_{calcd} values of **2** and **6** are similar to each other (vide supra).

Optoelectronic Properties. Figure 4 shows the electronic absorption spectra of **2**–**6** in CH_2Cl_2; the photograph of solutions of **2**–**6** in CH_2Cl_2 is shown in Figure S7. All

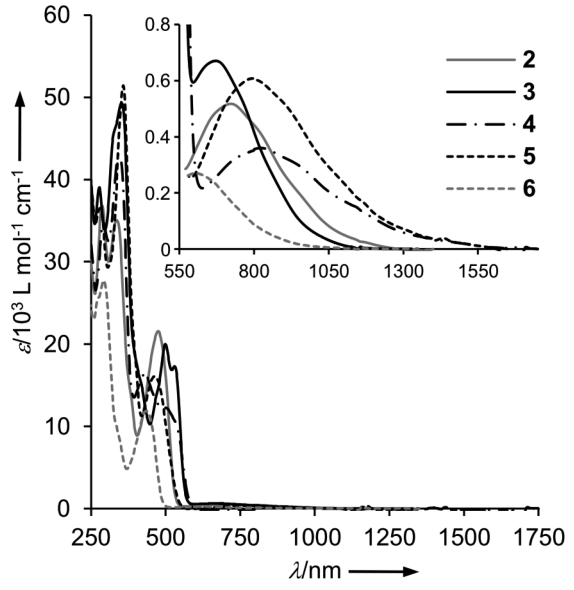

Figure 4. Electronic absorption spectra of **2**–**6** in CH_2Cl_2 at RT. (Inset) Long-wavelength, low-intensity absorptions ascribed to the symmetry-forbidden HOMO–LUMO transitions.

DOI: 10.1021/acs.joc.6b01409
J. Org. Chem. 2016, 81, 7700–7710

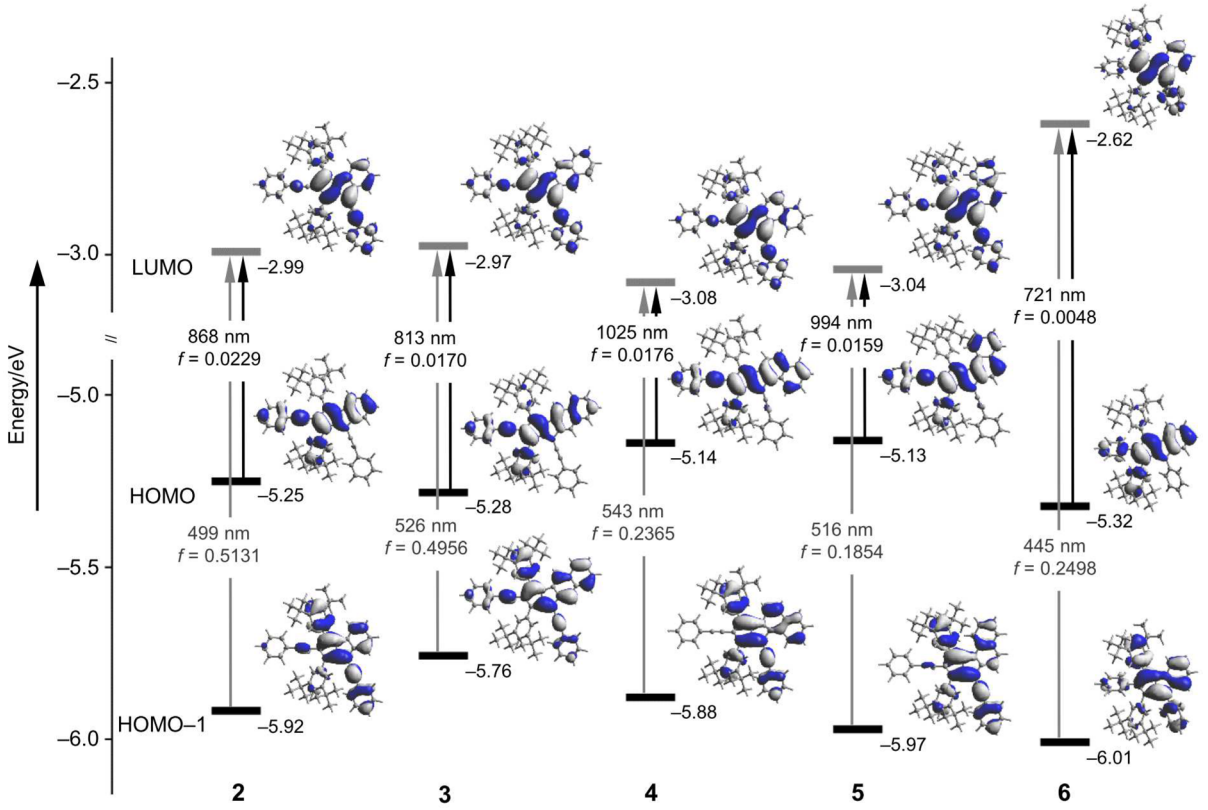

Figure 5. Calculated frontier molecular orbital profiles and energy diagrams of **2**–**6** at the PBE0/6-311G(d,p)//PBE0/6-31G(d) level and their lowest and second lowest energy transitions estimated by TD-DFT calculations at the PBE0/6-31G(d)//PBE0/6-31G(d) level.

compounds feature weak, broad low-energy absorptions with the longest wavelength absorption maxima (λ_{max}) between 606 and 822 nm in addition to two distinct absorptions in the 250–350 and 350–550 nm regions.[43] The end absorptions extend into the NIR region (over 1000 nm) without exception. We performed the single-point calculations of **2**–**6** at the PBE0/6-311G(d,p)//PBE0/6-31G(d) level, and the calculated surfaces of the selected frontier molecular orbitals (i.e., HOMO−1, HOMO, and LUMO) are depicted in Figure 5. The pentalene moieties of **2**–**6** largely contribute to their HOMO−1s, HOMOs, and LUMOs. Both the HOMOs and the LUMOs are of pseudo *ungerade*, while the HOMO−1s are of pseudo *gerade*. Hence, the longest absorption bands of **2**–**6** are reasonably assigned as the symmetrically forbidden HOMO → LUMO transitions as seen for $4n\pi$ electron systems; the transition dipole moments in the HOMO → LUMO transitions are extremely small (Figure S15). By contrast, the second longest absorptions are assignable to the symmetrically allowed HOMO−1 → LUMO transitions. The time-dependent (TD)-DFT calculations at the PBE0/6-31G(d) level nicely supported these assignments in light of the oscillator strength (f) (Figure 5 and Table S1); the f values of the HOMO → LUMO transitions (0.0048–0.0229) of **2**–**6** are much lower than those of the corresponding HOMO−1 → LUMO transitions (0.1854–0.5131).

Pentalene **2** exhibits the remarkably red-shifted longest λ_{max} relative to **6** by 116 nm (**2**: λ_{max} = 722 nm, ε = 510 L mol^{-1} cm^{-1}. **6**: λ_{max} = 606 nm, ε = 270 L mol^{-1} cm^{-1}), indicating the effective extension of π conjugation by the ethynylene units in **2**. As compared to **2**, the λ_{max} value of **3** is blue shifted by 51 nm despite the extension of the PCH framework (**3**: λ_{max} = 671 nm, ε = 670 L mol^{-1} cm^{-1}). On the contrary, the λ_{max} values of **4** and **5** are red shifted by 100 and 74 nm, respectively, relative to that of **2** (**4**: λ_{max} = 822 nm, ε = 360 L mol^{-1} cm^{-1}. **5**: λ_{max} = 796 nm, ε = 610 L mol^{-1} cm^{-1}). These findings demonstrate that the annulation at the 2,3 positions of naphthalene to the pentalene moiety increases the HOMO–LUMO gap relative to the benzannulation, whereas that at the 1,2 positions of naphthalene decreases the energy gap. The TD-DFT-calculated longest absorption maxima (λ_{max}^{calcd}) of **2**–**6** become red shifted in order of **6** < **3** < **2** < **5** ≈ **4** (Figure 5), and thus, the quantum chemical calculations reproduced well the experimental spectroscopic results in a qualitative manner.

Figure 6 shows the plot of the optical gaps (ΔE_{opt}), which are defined as the energies corresponding to the λ_{max} values, against the $NICS(1.7)_{\pi ZZ}^{avg.(X\text{-}ray)}$ values in **2**–**5**. Interestingly, the decrease in the ΔE_{opt} values is clearly correlated with the increase in the $NICS(1.7)_{\pi ZZ}^{avg.(X\text{-}ray)}$ values.[44] Given the fact that the $NICS(1.7)_{\pi ZZ}^{avg.(X\text{-}ray)}$ values in **2**–**5** increase with decreasing the $\alpha_{X\text{-}ray}$ values, one could argue that the increase in the bond order of the [5,6] junction enhances the 8π antiaromaticity and thus decreases the HOMO–LUMO gap.

Electrochemical Properties. We carried out cyclic voltammetry (CV) experiments on **2**–**6** in *o*-DCB (0.1 mol L^{-1} *n*-Bu_4NPF_6) to investigate their electrochemical properties. As shown in Figure 7, compounds **2**–**6** displayed amphoteric redox behavior within the available potential window; the oxidation potentials (E_{pa}) and reduction potentials (E_{pc}) versus ferrocenium/ferrocene (Fc^+/Fc) are summarized in Table 1. All pentalenes experienced two 1e$^-$ oxidation steps and two 1e$^-$ reduction steps. The first oxidation and reduction waves are reversible or quasi-reversible, indicating that the electrochemically generated radical–cationic and radical–anionic species are essentially stable. On the other hand, the second oxidation and

DOI: 10.1021/acs.joc.6b01409
J. Org. Chem. 2016, 81, 7700–7710

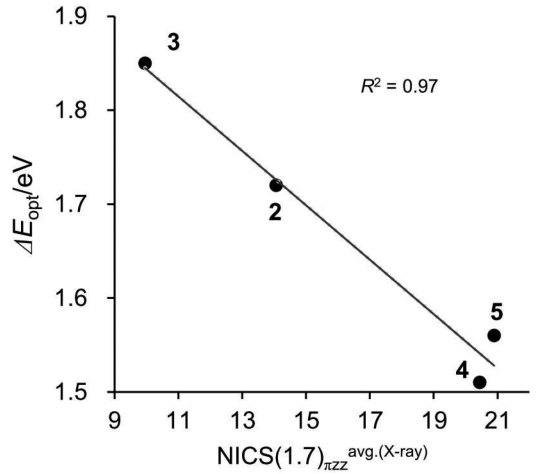

Figure 6. Plot of the ΔE_{opt} values as a function of the $NICS(1.7)_{\pi zz}^{avg.(X\text{-}ray)}$ values for **2**–**5**. NICS value for **3** is the average of those of $\mathbf{3}_1$ and $\mathbf{3}_2$.

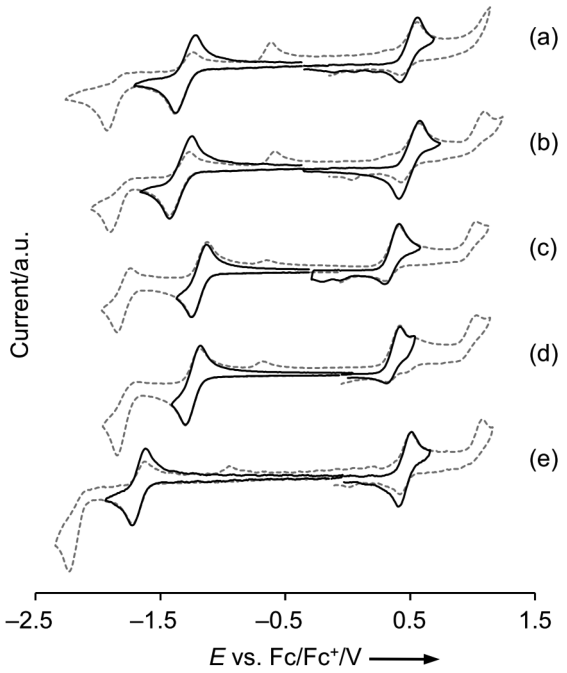

Figure 7. Cyclic voltammograms of (a) **2**, (b) **3**, (c) **4**, (d), **5**, and (e) **6** measured at a scan rate 100 mV s^{-1} in *o*-DCB (0.1 mol L^{-1} *n*-Bu_4NPF_6) at RT.

reduction waves are irreversible in general; the second reduction wave of **4** is exceptionally quasi-reversible. This illustrates that the dicationic and dianionic species are unstable except for the dianion of **4** under the conditions applied.

Both the first oxidation potential (E_{pa}^{1}) and the first reduction potential (E_{pc}^{1}) of **2** are positively shifted as compared to those for **6** (Table 1) owing to the electron-withdrawing ability of an ethynylene unit. The E_{pc}^{1} value is more positively shifted than the E_{pa}^{1} value, and thereby the difference (ΔE_{redox}, i.e. the electrochemical gap) between the E_{pa}^{1} and E_{pc}^{1} values of **2** becomes smaller than that of **6** (1.94 (**2**) and 2.22 V (**6**)). The E_{pa}^{1} value of **3** is positively shifted relative to that of **2**, while the values of **4** and **5** are negatively shifted. By contrast, the E_{pc}^{1} value of **3** negatively shifts compared to that of **2**, while the values of **4** and **5** positively

Table 1. Optical[a] and Electrochemical Data[b] for 2–6

	λ_{max}[c] [nm]	E_{pa}[d] [V]	E_{pc}[e] [V]	ΔE_{opt}[f] [eV]	ΔE_{redox}[g] [V]
2	722	+0.55[h]	−1.39[i]	1.72	1.94
		+1.13[j]	−1.93[j]		
3	671	+0.58[i]	−1.43[i]	1.85	2.01
		+1.09[j]	−1.91[j]		
4	822	+0.41[i]	−1.25[i]	1.51	1.66
		+1.03[j]	−1.85[h]		
5	796	+0.42[h]	−1.30[i]	1.56	1.72
		+1.03[j]	−1.84[j]		
6	606	+0.50[i]	−1.72[i]	2.05	2.22
		+1.07[j]	−2.23[j]		

[a]In CH_2Cl_2. [b]In *o*-DCB (0.1 mol L^{-1} *n*-Bu_4NPF_6). Scan rate 100 mV s^{-1}. [c]The longest absorption maxima. [d]Oxidation peak potentials. [e]Reduction peak potentials. [f]The optical gap, ΔE_{opt}, is defined as the energy corresponding to the λ_{max}. [g]The electrochemical gap, ΔE_{redox}, is defined as the potential difference between E_{pa} and E_{pc}. [h]Quasi-reversible wave. [i]Reversible wave. [j]Irreversible wave. DPV data are summarized in Table S2 in the Supporting Information.

shift. Consequently, as compared to **2**, compound **3** has a large ΔE_{redox} value, whereas **4** and **5** have small ΔE_{redox} values (2.01 (**3**), 1.66 (**4**), and 1.72 V (**5**)). These results clearly indicate that when compared with the benzannulation, the annulation at the 2,3 positions of naphthalene lowers the HOMO level and elevates the LUMO level to increase the HOMO–LUMO gap, and contrastingly, the annulation at the 1,2 positions elevates the HOMO level and lowers the LUMO level to decrease the energy gap. The plot of the ΔE_{opt} values against the ΔE_{redox} values in **2**–**6** shows a linear correlation (Figure S10), supporting that the same orbitals, namely HOMO and LUMO, are involved in both the optical and the electrochemical gaps.

Figure 8 shows plots of the E_{pa}^{1} and E_{pc}^{1} values against the $NICS(1.7)_{\pi ZZ}^{avg.(X\text{-}ray)}$ values for **2**–**5**. Noticeably, both E_{pa}^{1} and

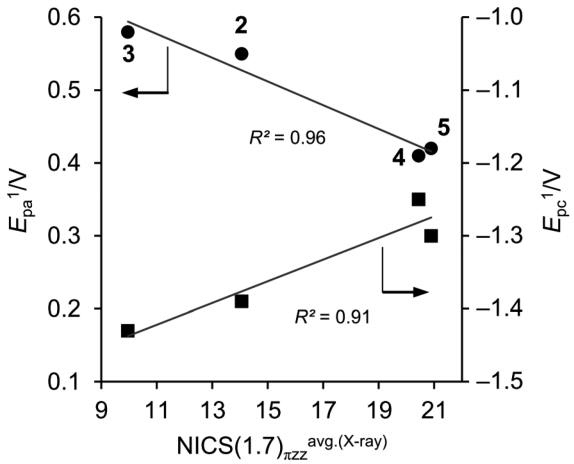

Figure 8. Plots of the E_{pa}^{1} (circle) and E_{pc}^{1} (square) values as a function of the $NICS(1.7)_{\pi zz}^{avg.(X\text{-}ray)}$ values. NICS value for **3** is the average of those of $\mathbf{3}_1$ and $\mathbf{3}_2$.

E_{pc}^{1} values have a strong correlation with the $NICS(1.7)_{\pi ZZ}^{avg.(X\text{-}ray)}$ values.[45] Taking the linear correlation between the $NICS(1.7)_{\pi ZZ}^{avg.(X\text{-}ray)}$ and the bond lengths ($\alpha_{X\text{-}ray}$) of the [5,6] junction into consideration (Figure 3), it can be concluded that the increase in the bond order of the [5,6] junction enhances the antiaromaticity and thereby leads

DOI: 10.1021/acs.joc.6b01409
J. Org. Chem. 2016, 81, 7700–7710

to both elevation of the HOMO level and lowering of the LUMO levels and decreases the HOMO−LUMO gaps.

CONCLUSION

We synthesized benzo- and naphthopentalenes **2**−**6** and investigated their structures, antiaromaticity, and optoelectronic and electrochemical properties experimentally and theoretically in detail. We disclosed that with increasing bond order of the carbon−carbon bond ([5,6] junction) shared by the pentalene and annulated aromatic moieties, the semilocal 8π antiaromaticity of the pentalene moiety is enhanced, and thereby the HOMO level elevates, while the LUMO level lowers; this work underlines the importance of the local structures on the global molecular properties in antiaromatic PCHs.[32] Introduction of the ethynylene units between the pentalene skeleton and the phenyl groups was found to bring about effective extension of π conjugation. The produced compounds showed intriguing vis−NIR absorptions and multiredox behaviors. We believe that the knowledge concerning relationships of the structures, antiaromaticity, and frontier molecular orbital levels presented herein will guide the development of new pentalene derivatives having interesting electronic and electrochemical properties. Further synthetic study on benzo- and naphthopentalenes is currently under way in our laboratory.

EXPERIMENTAL SECTION

General Procedure for the Synthesis of Pentalenequinone Derivatives. A mixture of 1,3-bis(3,5-di-*tert*-butylphenyl)propan-2-one (**7**) (1 equiv) and ninhydrin derivative (1 equiv) in EtOH or 1-butanol was degassed with argon for 30 min. The resulting mixture was warmed to 75 (EtOH) or 95 °C (1-butanol), and aqueous tetrabutylammonium hydroxide (40%, 0.3 equiv) was added slowly. After the mixture was heated for 1 (EtOH) or 2 h (1-butanol), the resulting mixture was concentrated under reduced pressure and the residue was dissolved with CH_2Cl_2. After the organic phase was separated, the aqueous phase was extracted with CH_2Cl_2. The combined organic phase was washed with water, dried over anhydrous $MgSO_4$, and concentrated under reduced pressure. The residue was subjected to column chromatography and washed with MeOH to give the desired pentalenequinone. An analytical sample was obtained by recycling GPC eluting with $CHCl_3$.

Preparation of ***11****.* 1,3-Bis(3,5-di-*tert*-butylphenyl)propan-2-one (**7**) (1.00 g, 2.30 mmol) was allowed to react with **8** (0.41 g, 2.30 mmol) in EtOH (9.2 mL) in the presence of aqueous tetrabutylammonium hydroxide (40%, 0.45 mL, 0.69 mmol) according to the general procedure for the synthesis of pentalenequinone derivatives. The obtained material was subjected to column chromatography (silica gel, toluene/hexane = 1:1) and washed with MeOH to give **11** (0.96 g, 1.72 mmol, 75%) as purple solids. Mp 211−213 °C. ^{1}H NMR (400 MHz, $CDCl_3$): δ 8.56 (2H, d, J = 1.7 Hz), 8.27−8.25 (1H, m), 8.12−8.10 (1H, m), 7.74−7.71 (2H, m), 7.60 (1H, t, J = 1.7 Hz), 7.58 (2H, d, J = 1.7 Hz), 7.52 (1H, t, J = 1.7 Hz), 1.45 (18H, s), 1.42 (18H, s). ^{13}C NMR (75 MHz, $CDCl_3$): δ 201.0, 185.4, 151.12, 151.05, 149.8, 143.5, 143.0, 138.6, 135.0, 133.1, 132.3, 130.0, 129.7, 126.0, 125.8, 125.0, 124.0, 123.0, 35.33, 35.24, 31.6 (21 signals out of 24 expected). UV−vis (CH_2Cl_2): λ_{max} (relative intensity) 262 (1.00), 353 (0.75), 555 nm (0.08). MALDI-TOF-MS (Dith, positive): m/z 557.2 (M^+). Anal. Calcd for $C_{40}H_{46}O_2$·0.03$CHCl_3$: C, 85.49; H, 8.25. Found: C, 85.48; H, 8.35.

Preparation of ***12****.* 1,3-Bis(3,5-di-*tert*-butylphenyl)propan-2-one (**7**) (381 mg, 0.88 mmol) was allowed to react with **9** (200 mg, 0.88 mmol) in 1-butanol (5 mL) in the presence of aqueous tetrabutylammonium hydroxide (40%, 0.17 mL, 0.26 mmol) according to the general procedure for the synthesis of pentalenequinone derivatives. The obtained material was subjected to column chromatography (silica gel, toluene/hexane = 1:1) and washed with MeOH to give **12** (101 mg, 0.17 mmol, 19%) as green solids. Mp 248−250 °C. ^{1}H NMR (400 MHz, $CDCl_3$): δ 8.84 (1H, s), 8.61 (1H, s) 8.57 (2H, d, J = 1.6 Hz), 8.10−8.07 (1H, m), 7.88−7.86 (1H, m), 7.71 (2H, d, J = 1.6 Hz), 7.67−7.63 (2H, m), 7.60 (1H, t, J = 1.6 Hz), 7.55 (1H, t, J = 1.6 Hz), 1.47 (18H, s), 1.46 (18H, s). ^{13}C NMR (75 MHz, $CDCl_3$): δ 201.4, 186.3, 151.13, 151.07, 150.5, 143.46, 139.6, 136.8, 135.2, 133.2, 131.6, 130.6, 130.3, 129.8, 129.4, 129.2, 128.7, 126.1, 125.9, 125.7, 124.0, 122.8, 122.1, 35.35, 35.29, 31.74, 31.64 (27 signals out of 28 expected). UV−vis (CH_2Cl_2): λ_{max} (relative intensity) 307 (0.92), 352 (1.00), 598 nm (0.06). MALDI-TOF-MS (Dith, positive): m/z 608.1 (M^+). Anal. Calcd for $C_{44}H_{48}O_2$·0.03$CHCl_3$: C, 86.35; H, 7.90. Found: C, 86.30; H, 8.06.

Preparation of ***13*** *and* ***14****.* 1,3-Bis(3,5-di-*tert*-butylphenyl)propan-2-one (**7**) (379 mg, 0.87 mmol) was allowed to react with **10** (203 mg, 0.89 mmol) in 1-butanol (5 mL) in the presence of aqueous tetrabutylammonium hydroxide (40%, 0.17 mL, 0.26 mmol) according to the general procedure for the synthesis of pentalenequinone derivatives. The obtained material was subjected to column chromatography (silica gel, toluene/hexane = 1:1) and washed with MeOH to give **13** (88 mg, 0.13 mmol, 17%) and **14** (20 mg, 33 μmol, 4%) as red solids. **13**: Mp 295−296 °C. ^{1}H NMR (400 MHz, $CDCl_3$): δ 9.64 (1H, d, J = 7.8 Hz), 8.57 (2H, d, J = 1.6 Hz), 8.18 (1H, d, J = 8.4 Hz), 8.11 (1H, d, J = 8.4 Hz), 7.97 (1H, d, J = 7.8 Hz), 7.82 (1H, dt, J = 7.8 and 0.8 Hz), 7.73 (1H, dt, J = 7.8 and 0.8 Hz), 7.62 (2H, d, J = 1.6 Hz), 7.59 (1H, t, J = 1.6 Hz), 7.54 (1H, t, J = 1.6 Hz), 1.46 (18H, s), 1.43 (18H, s). ^{13}C NMR (75 MHz, $CDCl_3$): δ 200.8, 185.7, 151.05, 151.01, 149.1, 143.8, 140.0, 139.3, 136.5, 135.5, 131.9, 130.1, 130.0, 129.9, 129.7, 129.40, 128.8, 126.5, 125.9, 125.5, 124.2, 123.5, 123.1, 121.7, 35.36, 35.27, 31.7 (27 signals out of 28 expected). UV−vis (CH_2Cl_2): λ_{max} (relative intensity) 295 (0.34), 255 (0.81), 372 nm (1.00). MALDI-TOF-MS (DHBA, positive): m/z 608.9 (M^+). Anal. Calcd for $C_{44}H_{48}O_2$: C, 86.80; H, 7.95. Found: C, 86.65; H, 7.95. **14**: Mp 287−289 °C. ^{1}H NMR (400 MHz, $CDCl_3$): δ 8.59 (2H, d, J = 1.8 Hz), 8.17 (1H, d, J = 8.4 Hz), 8.11 (1H, d, J = 8.4 Hz), 7.97 (1H, d, J = 8.0 Hz), 7.63−7.57 (4H, m), 7.30 (2H, d, J = 1.8 Hz), 7.20 (1H, dt, J = 7.8 and 1.2 Hz), 1.44 (18H, s), 1.33 (18H, s). ^{13}C NMR (75 MHz, $CDCl_3$): δ 201.6, 184.9, 151.1, 150.8, 149.0, 144.8, 144.5, 139.0, 137.1, 135.6, 131.8, 131.6, 130.0, 129.6, 129.4, 129.0, 128.1, 126.0, 125.7, 125.3, 123.3, 120.3, 35.4, 35.1, 31.65, 31.59 (26 signals out of 28 expected). UV−vis (CH_2Cl_2): λ_{max} (relative intensity) 255 (1.00), 322 (0.53), 379 nm (0.92). MALDI-TOF-MS (DHBA, positive): m/z 608.6 (M^+). Anal. Calcd for $C_{44}H_{48}O_2$·0.03$CHCl_3$: C, 86.35; H, 7.90. Found: C, 86.34; H, 8.05. The structures of **13** and **14** were undoubtedly identified with 2D NMR (HMBC and NOESY) spectroscopy.

General Procedure for the Synthesis of Pentalene Derivatives. A hexane solution of *n*-BuLi (1.6 mol L^{-1}, 0.55 mL, 0.88 mmol) was added dropwise to a solution of ethynylbenzene (0.10 mL, 0.91 mmol) in Et_2O or THF (8 mL) at 0 °C under argon atmosphere. The mixture was stirred at 0 °C for 1 h to afford fresh (2-phenylethynyl) lithium solution. This solution (4.0−8.3 equiv) was added dropwise to a solution of pentalenequinone derivative (1 equiv) in Et_2O at −78 °C, benzene at room temperature, or THF at −78 °C. The mixture was stirred at room temperature for 4 h. After the reaction was quenched by adding wet Et_2O and ice−water at 0 or −78 °C, the organic phase was separated and the aqueous phase was extracted with CH_2Cl_2. The combined organic phase was dried over anhydrous $MgSO_4$ and concentrated under reduced pressure to give crude diol (diastereomer mixture), which was used in the next reduction reaction without purification. A solution of the crude diol in THF was degassed with argon for 30 min. $SnCl_2$·$2H_2O$ (1.6−5.9 equiv) was added, and the mixture was stirred at 45 °C for 1.5−18 h. After addition of water, the organic phase was separated and the aqueous phase was extracted with CH_2Cl_2. The combined organic phase was dried over anhydrous $MgSO_4$ and concentrated under reduced pressure. The residue was purified by column chromatography and washed with MeOH to give the desired pentalene. An analytical sample was obtained by recycling GPC eluting with $CHCl_3$.

Preparation of ***2****.* Pentalenequinone **11** (100 mg, 0.179 mmol) in Et_2O (10 mL) was allowed to react with the freshly prepared (2-phenylethynyl)lithium (0.72 mmol) Et_2O solution to give crude diol

DOI: 10.1021/acs.joc.6b01409
J. Org. Chem. 2016, 81, 7700−7710

15 (124 mg) according to the general procedure for the synthesis of pentalene derivatives; the reaction was quenched at 0 °C. The crude diol **15** was treated with $SnCl_2{\cdot}2H_2O$ (65 mg, 0.288 mmol) in THF (20 mL) at 45 °C for 18 h. The obtained material was subjected to column chromatography (silica gel, CH_2Cl_2/hexane = 1:6) and washed with MeOH to give **2** (28 mg, 38.4 μmol, 21%) as green solids. Mp 180−181 °C. ^{1}H NMR (400 MHz, $CDCl_3$): δ 7.66 (2H, d, *J* = 1.7 Hz), 7.59 (2H, d, *J* = 1.7 Hz), 7.46 (1H, t, *J* = 1.7 Hz), 7.39 (1H, t, *J* = 1.7 Hz), 7.34−7.20 (10H, m), 7.05−7.01 (2H, m), 6.84−6.77 (2H, m), 1.35 (18H, s), 1.28 (18H, s). ^{13}C NMR (150 MHz, $CDCl_3$): δ 153.0, 150.2, 149.9, 148.9, 144.0, 143.2, 138.3, 136.0, 132.9, 132.6, 132.5, 131.6, 129.5, 129.3, 128.7, 128.4, 128.1, 127.25, 127.19, 123.7, 123.44, 123.41, 123.0, 122.9, 122.60, 122.57, 120.4, 104.9, 99.6, 88.0, 85.1, 35.2, 35.0, 31.69, 31.64 (35 signals out of 36 expected). UV−vis−NIR (CH_2Cl_2): λ_{max} (ε) 288 (36 800), 336 (35 000), 474 (21 600), 722 nm (510). MALDI-TOF-MS (Dith, positive): *m*/*z* 728.6 (M^+). HR-FAB-MS (NBA, positive): *m*/*z* calcd for $C_{56}H_{56}^+$ 728.4382; found 728.4380 (M^+).

Preparation of ***3***. Pentalenequinone **12** (100 mg, 0.164 mmol) in benzene (10 mL) was allowed to react with the freshly prepared (2-phenylethynyl)lithium (0.66 mmol) Et_2O solution to give crude diol **16** (157 mg) according to the general procedure for the synthesis of pentalene derivatives; the reaction was quenched at 0 °C. The crude diol **16** was treated with $SnCl_2{\cdot}2H_2O$ (218 mg, 0.965 mmol) in THF (20 mL) at 45 °C for 18 h. The obtained material was purified by column chromatography (silica gel, CH_2Cl_2/hexane = 1:6) and washed with MeOH to give **3** (44 mg, 38.0 μmol, 34%) as red solids. Mp 200−201 °C. ^{1}H NMR (600 MHz, $CDCl_3$): δ 7.72 (2H, d, *J* = 1.8 Hz), 7.68 (2H, d, *J* = 1.8 Hz), 7.59−7.58 (1H, m), 7.55 (1H, s), 7.49 (1H, t, *J* = 1.8 Hz), 7.46 (1H, s), 7.41 (1H, t, *J* = 1.8 Hz), 7.39−7.34 (2H, m), 7.31−7.29 (4H, m), 7.27−7.23 (7H, m), 1.41 (18H, s), 1.29 (18H, s). ^{13}C NMR (150 MHz, $CDCl_3$): δ 155.3, 150.3, 149.9, 147.6, 141.3, 140.4, 136.9, 135.3, 133.6, 133.2, 132.7, 132.6, 132.5, 131.7, 130.7, 129.6, 129.3, 128.6, 128.4, 128.22, 128.15, 127.3, 127.1, 126.3, 123.7, 123.5, 123.0, 122.9, 122.7, 122.57, 122.54, 119.1, 105.1, 100.3, 88.2, 84.9, 35.2, 35.0, 31.8, 31.7. UV−vis−NIR (CH_2Cl_2): λ_{max} (ε) 278 (39 000), 352 (49 300), 499 (20 000), 530 (17 300), 671 nm (670). MALDI-TOF-MS (Dith, positive): *m*/*z* 778.3 (M^+). HR-FAB-MS (NBA, positive): *m*/*z* calcd for $C_{60}H_{58}^+$ 778.4538; found 778.4534 (M^+).

Preparation of ***4***. Pentalenequinone **13** (30 mg, 49.3 μmol) in THF (8 mL) was allowed to react with the freshly prepared (2-phenylethynyl)lithium (0.41 mmol) THF solution to give crude diol **17** (54 mg) according to the general procedure for the synthesis of pentalene derivatives; the reaction was quenched at −78 °C. The crude diol **17** was treated with $SnCl_2{\cdot}2H_2O$ (57 mg, 0.25 mmol) in THF (12 mL) at 45 °C for 1.5 h. The obtained material was purified by column chromatography (silica gel, CH_2Cl_2/hexane = 1:6) and washed with MeOH to give **4** (3 mg, 3.9 μmol, 8%) as red solids. Mp 230−232 °C. ^{1}H NMR (400 MHz, $CDCl_3$): δ 8.78 (1H, d, *J* = 8.7 Hz), 7.62 (2H, d, *J* = 1.8 Hz), 7.60 (2H, d, *J* = 1.8 Hz), 7.50 (1H, d, *J* = 8.7 Hz), 7.49 (1H, d, *J* = 1.8 Hz), 7.40 (1H, d, *J* = 1.8 Hz), 7.31−7.27 (3H, m), 7.23−7.16 (8H, m), 7.15 (1H, d, *J* = 8.4 Hz), 6.96 (2H, dd *J* = 8.4 and 1.2 Hz), 1.37 (18H, s), 1.27 (18H, s). ^{13}C NMR (150 MHz, $CDCl_3$): δ 156.1, 150.3, 149.9, 147.0, 146.3, 141.2, 139.2, 135.7, 134.4, 132.6, 132.4, 132.2, 131.5, 130.7, 129.7, 129.5, 128.9, 128.3, 128.1, 128.0, 127.8, 127.0, 124.9, 124.0, 123.8, 123.4, 123.0, 123.0, 122.7, 122.5, 119.6, 105.1, 99.1, 88.3, 87.6, 35.2, 35.0, 31.67, 31.60 (39 signals out of 40 expected). UV−vis−NIR (CH_2Cl_2): λ_{max} (ε) 291 (34 800), 343 (43 100), 431 (16 600), 499 (12 300), 822 nm (360). MALDI-TOF-MS (Dith, positive): *m*/*z* 779.4 [$(M + H)^+$]. HR-FAB-MS (NBA, positive): *m*/*z* calcd for $C_{60}H_{58}^+$ 778.4538; found 778.4537 (M^+).

Preparation of ***5***. Pentalenequinone **14** (30 mg, 49.3 μmol) in THF (8 mL) was allowed to react with the freshly prepared (2-phenylethynyl)lithium (0.41 mmol) THF solution to give crude diol **18** (63 mg) according to the general procedure for the synthesis of pentalene derivatives; the reaction was quenched at −78 °C. The crude diol **18** was treated with $SnCl_2{\cdot}2H_2O$ (57 mg, 0.25 mmol) in THF (10 mL) at 45 °C for 1.5 h. The obtained material was purified by column chromatography (silica gel, CH_2Cl_2/hexane = 1:6) and washed with MeOH to give **5** (14 mg, 18.0 μmol, 29%) as dark yellow solids. Mp 235−237 °C. ^{1}H NMR (400 MHz, $CDCl_3$): δ 7.67 (2H, d, *J* = 1.9 Hz), 7.50 (1H, t, *J* = 1.9 Hz), 7.44 (1H, d, *J* = 8.4 Hz), 7.39 (1H, t, *J* = 1.9 Hz), 7.36 (2H, d, *J* = 1.9 Hz), 7.34−7.28 (4H, m), 7.25−7.15 (6H, m), 7.06−7.02 (3H, m), 6.73−6.67 (2H, m), 1.29 (18H, s), 1.28 (18H, s). ^{13}C NMR (150 MHz, $CDCl_3$): δ 154.6, 150.6, 150.0, 147.5, 146.8, 142.7, 141.7, 135.4, 134.1, 133.9, 132.5, 132.2, 131.5, 130.0, 129.5, 128.7, 128.4, 128.09, 128.03, 127.98, 127.8, 126.7, 126.2, 125.7, 123.7, 123.2, 123.1, 122.6, 122.1, 120.7, 104.6, 99.7, 88.0, 85.2, 35.03, 35.01, 31.6 (37 signals out of 40 expected). UV−vis−NIR (CH_2Cl_2): λ_{max} (ε) 280 (36 500), 358 (51 400), 463 (16 100), 796 nm (610). MALDI-TOF-MS (Dith, positive): *m*/*z* 778.4 (M^+). HR-FAB-MS (NBA, positive): *m*/*z* calcd for $C_{60}H_{58}^+$ 778.4538; found 778.4544 (M^+).

Preparation of ***6***. A cyclohexane/Et_2O solution of phenyllithium (1.05 mol L^{-1}, 0.70 mL, 0.74 mmol) was added dropwise to a solution of **11** (100 mg, 0.18 mmol) in benzene (10 mL) at room temperature under argon atmosphere. The mixture was stirred at room temperature for 30 min. After the reaction was quenched by adding wet Et_2O (20 mL) and ice−water (20 mL) at 0 °C, the organic phase was separated and the aqueous phase was extracted with CH_2Cl_2. The combined organic phase was dried over anhydrous $MgSO_4$ and concentrated under reduced pressure to give crude diol **19** (155 mg); the structure of **20** is shown in Scheme S2 in the Supporting Information. $SnCl_2{\cdot}2H_2O$ (369 mg, 1.63 mmol) was dissolved with a mixture of HCl (3.2 mL) and AcOH (1.6 mL). A solution of the crude **19** (155 mg) in 1,4-dioxane (3.2 mL) was slowly added dropwise, and the resulting mixture was stirred at room temperature for 4 h. The precipitate was collected by filtration and washed with water. After the solid was dissolved with CH_2Cl_2 (20 mL), the resulting solution was dried over anhydrous $MgSO_4$ and concentrated under reduced pressure. The residue was purified by column chromatography (silica gel, CH_2Cl_2/hexane = 1:6) to give **6** (9 mg, 13.2 μmol, 8%) as green solids. Mp 231−233 °C. ^{1}H NMR (400 MHz, $CDCl_3$): δ 7.17−7.13 (3H, m), 7.08−7.01 (6H, m), 6.96 (3H, d, *J* = 1.6 Hz), 6.78−6.66 (6H, m), 6.63 (2H, d, *J* = 1.6 Hz), 1.17 (18H, s), 0.95 (18H, s). ^{13}C NMR (75 MHz, $CDCl_3$): δ 149.62, 149.55, 149.3, 148.6, 147.0, 144.8, 138.8, 137.2, 136.0, 135.5, 133.1, 132.99, 132.86, 130.0, 129.3, 128.8, 128.6, 128.0, 127.4, 126.6, 126.4, 124.0, 123.5, 123.3, 121.8, 120.8, 120.5, 34.9, 34.4, 31.4, 31.2 (31 signals out of 32 expected). UV−vis−NIR (CH_2Cl_2): λ_{max} (ε) 292 (27 700), 436 (11 900), 606 nm (270). MALDI-TOF-MS (Dith, positive): *m*/*z* 680.3 (M^+). HR-FAB-MS (NBA, positive): *m*/*z* calcd for $C_{52}H_{56}^+$ 680.4382, found 680.4379 (M^+).

■ ASSOCIATED CONTENT

Supporting Information

The Supporting Information is available free of charge on the ACS Publications website at DOI: 10.1021/acs.joc.6b01409.

General experimental methods, complete X-ray crystallographic, electronic absorption spectroscopic, electrochemical, and theoretical data, and ^{1}H and ^{13}C NMR spectra of new compounds (PDF)

Crystallographic information on **2** (CIF)

Crystallographic information on **3** (CIF)

Crystallographic information on **4** (CIF)

Crystallographic information on **5** (CIF)

■ AUTHOR INFORMATION

Corresponding Author

*E-mail: nakamura@gunma-u.ac.jp. Phone: +81 277 30 1310. Fax: +81 277 30 1314.

Notes

The authors declare no competing financial interest.

DOI: 10.1021/acs.joc.6b01409
J. Org. Chem. 2016, 81, 7700−7710

■ ACKNOWLEDGMENTS

This work was financially supported by Grants-in-Aid for Scientific Research from MEXT, Japan (Nos. 15K05415, 15K05416, 25870112), a research grant from the Kurata Memorial Hitachi Science and Technology Foundation, and a Showa Denko Award in The Society of Synthetic Organic Chemistry, Japan. This work was performed under the Cooperative Research Program of "Network Joint Research Center for Materials and Devices" (Kyushu University). Quantum chemical calculations were performed in the Research Center for Computational Science, Japan. We thank Prof. Soichiro Kyushin (Gunma University) for generous permission to use the UV−vis−NIR spectroscopy.

■ REFERENCES

(1) Harvey, R. G. *Polycyclic Aromatic Hydrocarbons*; Wiley-VCH: Weinheim, Germany, 1997.
(2) (a) Breslow, R. *Acc. Chem. Res.* **1973**, *6*, 393. (b) Krygowski, T. M.; Cyrañski, M. K.; Czarnocki, Z.; Häfelinger, G.; Katritzky, A. R. *Tetrahedron* **2000**, *56*, 1783.
(3) Minkin, V. I.; Glukhovtsev, M. N.; Simkin, B. Y. *Aromaticity and Antiaromaticity: Electronic and Structural Aspects*; Wiley: New York, 1994.
(4) Rudebusch, G. E.; Haley, M. M. In *Polycyclic Arenes and Heteroarenes: Synthesis, Properties, and Applications*; Miao, Q., Ed.; Wiley-VCH: Weinheim, 2015.
(5) For some recent examples, see: (a) Chase, D. T.; Fix, A. G.; Kang, S. J.; Rose, B. D.; Weber, C. D.; Zhong, Y.; Zakharov, L. N.; Lonergan, M. C.; Nuckolls, C.; Haley, M. M. *J. Am. Chem. Soc.* **2012**, *134*, 10349. (b) Nishida, J.-i.; Tsukaguchi, S.; Yamashita, Y. *Chem. - Eur. J.* **2012**, *18*, 8964. (c) Nishinaga, T.; Ohmae, T.; Aita, K.; Takase, M.; Iyoda, M.; Arai, T.; Kunugi, Y. *Chem. Commun.* **2013**, *49*, 5354.
(6) (a) Hafner, K. *Nachr. Chem., Tech. Lab.* **1980**, *28*, 222. (b) Hopf, H. *Angew. Chem., Int. Ed.* **2013**, *52*, 12224.
(7) Inter alia: (a) Le Goff, E. *J. Am. Chem. Soc.* **1962**, *84*, 3975. (b) Hafner, K.; Süss, H.-U. *Angew. Chem., Int. Ed. Engl.* **1973**, *12*, 575. (c) Bally, T.; Chai, S.; Neuenschwander, M.; Zhu, Z. *J. Am. Chem. Soc.* **1997**, *119*, 1869.
(8) Brand, K. *Ber. Dtsch. Chem. Ges.* **1912**, *45*, 3071.
(9) Kawase, T.; Konishi, A.; Hirao, Y.; Matsumoto, K.; Kurata, H.; Kubo, T. *Chem. - Eur. J.* **2009**, *15*, 2653.
(10) Levi, Z. U.; Tilley, T. D. *J. Am. Chem. Soc.* **2009**, *131*, 2796.
(11) The first synthesis of dibenzo[*a*,*e*]pentalene derivatives by Pd-catalyzed dimerization of *o*-alkynylhaloarene was reported by Youngs and co-workers: Chakraborty, M.; Tessier, C. A.; Youngs, W. J. *J. Org. Chem.* **1999**, *64*, 2947.
(12) Kawase, T.; Fujiwara, T.; Kitamura, C.; Konishi, A.; Hirao, Y.; Matsumoto, K.; Kurata, H.; Kubo, T.; Shinamura, S.; Mori, H.; Miyazaki, E.; Takimiya, K. *Angew. Chem., Int. Ed.* **2010**, *49*, 7728.
(13) Yin, X.; Li, Y.; Zhu, Y.; Kan, Y.; Li, Y.; Zhu, D. *Org. Lett.* **2011**, *13*, 1520.
(14) (a) Xu, F.; Peng, L.; Orita, A.; Otera, J. *Org. Lett.* **2012**, *14*, 3970. (b) Xu, F.; Peng, L.; Shinohara, K.; Nishida, T.; Wakamatsu, K.; Uejima, M.; Sato, T.; Tanaka, K.; Machida, N.; Akashi, H.; Orita, A.; Otera, J. *Org. Lett.* **2015**, *17*, 3014.
(15) Maekawa, T.; Segawa, Y.; Itami, K. *Chem. Sci.* **2013**, *4*, 2369.
(16) Zhao, J.; Oniwa, K.; Asao, N.; Yamamoto, Y.; Jin, T. *J. Am. Chem. Soc.* **2013**, *135*, 10222.
(17) (a) Chen, C.; Harhausen, M.; Liedtke, R.; Bussmann, K.; Fukazawa, A.; Yamaguchi, S.; Petersen, J. L.; Daniliuc, C. G.; Fröhlich, R.; Kehr, G.; Erker, G. *Angew. Chem., Int. Ed.* **2013**, *52*, 5992. (b) Chen, C.; Harhausen, M.; Fukazawa, A.; Yamaguchi, S.; Fröhlich, R.; Daniliuc, C. G.; Petersen, J. L.; Kehr, G.; Erker, G. *Chem. - Asian J.* **2014**, *9*, 1671.
(18) (a) Nakano, M.; Osaka, I.; Takimiya, K.; Koganezawa, T. *J. Mater. Chem. C* **2014**, *2*, 64. (b) Nakano, M.; Osaka, I.; Takimiya, K. *J. Mater. Chem. C* **2015**, *3*, 283.
(19) (a) Shen, J.; Yuan, D.; Qiao, Y.; Shen, X.; Zhang, Z.; Zhong, Y.; Yi, Y.; Zhu, X. *Org. Lett.* **2014**, *16*, 4924. (b) Liu, C.; Xu, S.; Zhu, W.; Zhu, X.; Hu, W.; Li, Z.; Wang, Z. *Chem. - Eur. J.* **2015**, *21*, 17016. (c) Li, C.; Liu, C.; Li, Y.; Zhu, X.; Wang, Z. *Chem. Commun.* **2015**, *51*, 693. (d) Shen, J.-J.; Shao, J.-Y.; Zhu, X.; Zhong, Y.-W. *Org. Lett.* **2016**, *18*, 256.
(20) (a) Dai, G.; Chang, J.; Zhang, W.; Bai, S.; Huang, K.-W.; Xu, J.; Chi, C. *Chem. Commun.* **2015**, *51*, 503. (b) Dai, G.; Chang, J.; Shi, X.; Zhang, W.; Zheng, B.; Huang, K.-W.; Chi, C. *Chem. - Eur. J.* **2015**, *21*, 2019.
(21) (a) Ried, W.; Freitag, D. *Tetrahedron Lett.* **1967**, *8*, 3135. (b) Ried, W.; Freitag, D. *Chem. Ber.* **1968**, *101*, 756. (c) Ried, W.; Schaefer, H.-J. *Synthesis* **1970**, *1970*, 142.
(22) Brown, R. F. C.; Choi, N.; Coulston, K. J.; Eastwood, F. W.; Wiersum, U. E.; Jenneskens, L. W. *Tetrahedron Lett.* **1994**, *35*, 4405.
(23) Dix, I.; Doll, C.; Hopf, H.; Jones, P. *Eur. J. Org. Chem.* **2002**, *2002*, 2547.
(24) Blake, M. E.; Bartlett; Jones, M., Jr. *J. Am. Chem. Soc.* **2003**, *125*, 6485.
(25) Shukla, B.; Tsuchiya, K.; Koshi, M. *J. Phys. Chem. A* **2011**, *115*, 5284.
(26) Comandini, A.; Malewicki, T.; Brezinsky, K. *J. Phys. Chem. A* **2012**, *116*, 2409.
(27) In contrast to dibenzo[*a*,*e*]pentalene, benzopentalene is highly reactive and thus dimerizes above −70 °C (ref 22).
(28) (a) Rivera-Fuentes, P.; Rekowski, M. v. W.; Schweizer, W. B.; Gisselbrecht, J.-P.; Boudon, C.; Diederich, F. *Org. Lett.* **2012**, *14*, 4066. (b) London, G.; von Wantoch Rekowski, M.; Dumele, O.; Schweizer, W. B.; Gisselbrecht, J.-P.; Boudon, C.; Diederich, F. *Chem. Sci.* **2014**, *5*, 965.
(29) Miao, S.; Brombosz, S. M.; Schleyer, P. v. R.; Wu, J. I.; Barlow, S.; Marder, S. R.; Hardcastle, K. I.; Bunz, U. H. F. *J. Am. Chem. Soc.* **2008**, *130*, 7339.
(30) Ohmae, T.; Nishinaga, T.; Wu, M.; Iyoda, M. *J. Am. Chem. Soc.* **2010**, *132*, 1066.
(31) Iida, A.; Sekioka, A.; Yamaguchi, S. *Chem. Sci.* **2012**, *3*, 1461.
(32) Cao, J.; London, G.; Dumele, O.; von Wantoch Rekowski, M.; Trapp, N.; Ruhlmann, L.; Boudon, C.; Stanger, A.; Diederich, F. *J. Am. Chem. Soc.* **2015**, *137*, 7178.
(33) Our synthetic protocols were modified for those for **1** (Scheme S1 in the Supporting Information).
(34) Diols **15**−**18** seem to be diastereomeric mixtures based on their ^{1}H NMR spectra.
(35) The Wiberg bond indexes of the [5,6] junction were calculated to be 1.277 for **2**, 1.178 for $\mathbf{3}_1$, 1.168 for $\mathbf{3}_2$, 1.350 for **4**, and 1.372 for **5** by natural bond orbital analyses at the PBE0/6-31G(d) level with the Gaussian 09 suite of program (ref 36).
(36) Frisch, M. J.; Trucks, G. W.; Schlegel, H. B.; Scuseria, G. E.; Robb, M. A.; Cheeseman, J. R.; Scalmani, G.; Barone, V.; Mennucci, B.; Petersson, G. A.; Nakatsuji, H.; Caricato, M.; Li, X.; Hratchian, H. P.; Izmaylov, A. F.; Bloino, J.; Zheng, G.; Sonnenberg, J. L.; Hada, M.; Ehara, M.; Toyota, K.; Fukuda, R.; Hasegawa, J.; Ishida, M.; Nakajima, T.; Honda, Y.; Kitao, O.; Nakai, H.; Vreven, T.; Montgomery, Jr., J. A.; Peralta, J. E.; Ogliaro, F.; Bearpark, M.; Heyd, J. J.; Brothers, E.; Kudin, K. N.; Staroverov, V. N.; Keith, T.; Kobayashi, R.; Normand, J.; Raghavachari, K.; Rendell, A.; Burant, J. C.; Iyengar, S. S.; Tomasi, J.; Cossi, M.; Rega, N.; Millam, J. M.; Klene, M.; Knox, J. E.; Cross, J. B.; Bakken, V.; Adamo, C.; Jaramillo, J.; Gomperts, R.; Stratmann, R. E.; Yazyev, O.; Austin, A. J.; Cammi, R.; Pomelli, C.; Ochterski, J. W.; Martin, R. L.; Morokuma, K.; Zakrzewski, V. G.; Voth, G. A.; Salvador, P.; Dannenberg, J. J.; Dapprich, S.; Daniels, A. D.; Farkas, Ö.; Foresman, J. B.; Ortiz, J. V.; Cioslowski, J.; Fox, D. J. *Gaussian 09*, Revision D.01; Gaussian, Inc.: Wallingford, CT, 2013.
(37) Chen, Z.; Wannere, C. S.; Corminboeuf, C.; Puchta, R.; Schleyer, P. v. R. *Chem. Rev.* **2005**, *105*, 3842.
(38) (a) Stanger, A. *J. Org. Chem.* **2006**, *71*, 883. (b) Stanger, A. *J. Org. Chem.* **2010**, *75*, 2281. (c) Gershoni-Poranne, R.; Stanger, A. *Chem. - Eur. J.* **2014**, *20*, 5673.

DOI: 10.1021/acs.joc.6b01409
J. Org. Chem. 2016, 81, 7700−7710

(39) Rahalkar, A.; Stanger, A. *Aroma*; http://schulich.technion.ac.il/Amnon_Stanger.htm.
(40) Almost no noticeable difference in the carbon−carbon bond lengths is observable in the outer 6-membered rings D of **3**−**5**. We investigated the aromaticity of the rings D of **3**−**5** by HOMA (harmonic oscillator model of aromaticity) analyses (ref 41). The HOMA values of $\mathbf{3}_1$, $\mathbf{3}_2$, **4**, and **5** are 0.83, 0.84, 0.83, and 0.75, respectively, and the difference in the aromaticity of the rings D is considered to be negligible.
(41) For a review on HOMA, see: Krygowski, T. M.; Cyrański, M. K. *Chem. Rev.* **2001**, *101*, 1385.
(42) It was pointed out that the aromaticity and antiaromaticity of annulenic compounds are highly dependent on their annulated aromatics. For some examples, see: (a) Walsgrove, T. C.; Sondheimer, F. *Tetrahedron Lett.* **1978**, *19*, 2719. (b) Boydston, A. J.; Haley, M. M.; Williams, R. V.; Armantrout, J. R. *J. Org. Chem.* **2002**, *67*, 8812. (c) Kato, S.-i.; Takahashi, N.; Tanaka, H.; Kobayashi, A.; Yoshihara, T.; Tobita, S.; Yamanobe, T.; Uehara, H.; Nakamura, Y. *Chem. - Eur. J.* **2013**, *19*, 12138.
(43) All of **2**−**6** are nonfluorescent in both the solution and the solid state.
(44) There is an obvious relationship between the $NICS(1.7)_{\pi ZZ}^{avg.(calcd)}$ and ΔE_{opt} values (Figure S8).
(45) Both the HOMO and the LUMO levels are linearly related to the $NICS(1.7)_{\pi ZZ}^{avg.(calcd)}$ values (Figure S12).

DOI: 10.1021/acs.joc.6b01409
J. Org. Chem. 2016, 81, 7700−7710